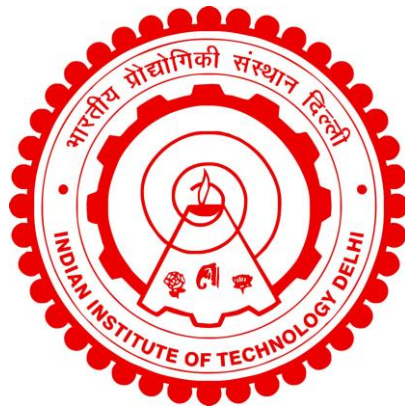


INVESTIGATION OF RETINAL BIOMARKERS FOR EARLY DETECTION OF VISUAL IMPAIRMENT

GEETHA PAVANI PAPPU



**DEPARTMENT OF ELECTRICAL ENGINEERING
INDIAN INSTITUTE OF TECHNOLOGY DELHI
FEBRUARY 2026**

© Indian Institute of Technology Delhi (IITD), New Delhi, 2026

**INVESTIGATION OF RETINAL BIOMARKERS FOR EARLY
DETECTION OF VISUAL IMPAIRMENT**

by

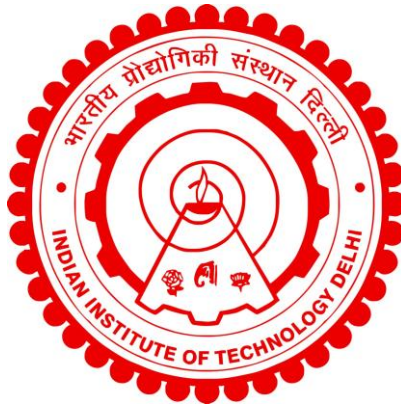
GEETHA PAVANI PAPPU

DEPARTMENT OF ELECTRICAL ENGINEERING

Submitted

in fulfilment of the requirements of the degree of Doctor of Philosophy

to the



INDIAN INSTITUTE OF TECHNOLOGY DELHI

February 2026

Dedicated to

My Family



Department of Electrical Engineering
Indian Institute of Technology Delhi
Hauz Khas, New Delhi, India-110016

CERTIFICATE

This is to certify that the thesis entitled “**INVESTIGATION OF RETINAL BIOMARKERS FOR EARLY DETECTION OF VISUAL IMPAIRMENT**”, submitted by **Ms. Geetha Pavani (2020EEZ8644)** to the Indian Institute of Technology Delhi, for the award of the degree of **Doctor of Philosophy** in Department of Electrical Engineering, is a record of the original, Bonafide research work carried out by him under our supervision and guidance. The thesis has reached the standards fulfilling the requirements of the regulations related to the award of the degree.

The results contained in this thesis have not been submitted in part or in full to any other University or Institute for the award of any degree or diploma to the best of our knowledge.

Prof. Tapan Kumar Gandhi

Electrical Engineering,
Indian Institute of Technology Delhi.

Date:

Place:

Prof. Birendra Biswal

Electronics and Communication Engineering,
Gayatri Vidya Parishad College of Engineering,
Visakhapatnam.

Date:

Place:

Acknowledgements

To begin with, I, Geetha Pavani, express the most sincere and profound gratitude to both supervisors, Dr. Tapan Kumar Gandhi and Dr. Birendra Biswal, for rendering unwavering support, guidance, and patience throughout the time of completion of the Ph.D. work. I thank you for infusing confidence, excitement, and inspiring me in my work through continuous encouragement and superb guidance. I will always be indebted to both of you for doing everything during the journey of completing the Ph.D.

The suggestions and the guidance provided by Dr. Tapan Kumar Gandhi Sir have enabled me to learn more knowledge beyond the classroom from my Ph.D. journey. It is my privilege to work with him and learned many aspects of Ph.D.

I am always grateful to Dr. Birendra Biswal, sir. You are the first person who taught me “what is research,” and you are the one who initially recognized my hidden strength and always pointed out my weaknesses, which helped to overcome and become what I am today. I still remember the first day of M.Tech, you made me see what I had never seen in my whole life. You have pushed my limits, and I could not have asked for a better advisor. I sincerely thank you from the bottom of my heart for your affection towards me.

I would like to thank my SRC committee members, Dr. Brijesh Lall, Dr. Sumantra Dutta Roy, and Dr. Amit Mehndiratta, for the beneficial feedback provided during the Ph.D. I would also like to thank the administrative staff of the Department of Electrical Engineering for their timely response and support for any necessary communication.

I would like to extend my sincere gratitude to Prof. Dr. A. B. Koteswara Rao, Principal, Gayatri Vidya Parishad College of Engineering (Autonomous), for providing an excellent ambiance along with supporting teaching faculty, staff, and lab facilities to work in the “Center for Medical Imaging Studies (CMIS)”. I also thank all the faculty of the Department of Electronics and Communication Engineering for their encouragement throughout my Ph.D. journey. I shall remain obliged to Prof. U.S.N. Murthy and his team of doctors from Gayatri Vidya Parishad Institute of Health Care and Medical Technology for sharing the data related to eye care.

I would also like to extend my deep sense of gratitude to Mrs. K. B. N. Manimala, CEO of “Simadri Surya Eye Hospital”, Nabarangpur, Odisha, for her constant encouragement and support for

carrying out research in the hospital and discussing the critical aspects of eye care with doctors during my Ph.D. journey.

I thank all my co-scholars from the Neurocomputing lab, IIT Delhi, Dr. Shefali, Raghav Dev, Dr. Sapna Mishra, Dr. Amit Bhongade, Ashirbad, and all others for their support, which made my Ph.D. journey more comfortable. I also thank members of the CMIS lab, mainly Sreekar Tankala, who helped me in learning Python coding and spent their valuable time throughout the day to solve the errors in the code. I thank all my best friends, Sai Bhanu Palli, Tejaswini Sai Aparna and well-wishers for their prayers and support.

In a final note, I would like to acknowledge both my mother and brother, who have always supported me in pursuing the most awaited lifelong dream of earning a Ph.D. I always believe that I have blessings of my father and he is with me in every moment to guide me in the right path. I am strong today because I am confident that you will always hold my hand if I fall. AMMA, all thanks to you for bringing me to Visakhapatnam and nurturing me to become an independent person. I wholeheartedly dedicate this thesis to you, without you, it would have been impossible to be what I am today.

Lastly, I would like to express gratitude to my husband and my In-law's family, though he came into my life in the last phase of my Ph.D. Journey. He constantly encouraged and supported to complete the work.

Finally, I thank everyone who have constantly supported and encouraged me directly or indirectly. This achievement is not mine alone, but a reflection of the kindness, faith, and encouragement I received throughout this journey.

Geetha Pavani Pappu

Abstract

This thesis focuses on the comprehensive investigation of retinal disorders, emphasizing early detection to prevent irreversible damage and vision loss. Diagnosing retinal diseases such as Glaucoma, Macular Edema (ME), Hypertensive Retinopathy (HR), Diabetic Retinopathy (DR), and Age-related Macular Degeneration (AMD) remains a significant challenge, particularly because early-stage manifestations are often subtle and difficult to detect. The growing prevalence of diabetes and hypertension has led to a rapid increase in retinal disorders, further straining healthcare systems already facing a shortage of expert ophthalmologists. In this context, recent advancements in automated medical image processing have emerged as promising solutions, reducing diagnostic time and minimizing human errors while supporting clinical decision-making.

The primary objective of this research is to develop deep learning–based frameworks capable of detecting both structural alterations and clinical indicators in retinal images to enable accurate and timely diagnosis. The study investigates multiple retinal components, including retinal vessel maps, Optic Disc (OD), Optic Cup (OC), and pathological features such as retinal fluids and drusen from Optical Coherence Tomography (OCT) scans. By integrating structural and pathological analysis, the proposed system aims to improve early-stage detection and patient outcomes.

Despite numerous existing studies, substantial research gaps remain in enhancing the robustness and decision-making capability of automated systems. The first major contribution of this work is the development of a novel multistage dual-decoder deep learning architecture named “Multistage DPIRef-Net.” This model performs precise segmentation of retinal blood vessels and further classifies them into arteries and veins to support accurate diagnosis. The architecture addresses limitations associated with pooling and striding operations by enhancing low-level feature representation, thereby preserving fine vascular details and reducing blurred boundaries. Extensive evaluations on publicly available benchmark datasets demonstrate the robustness and generalization ability of the proposed vessel segmentation framework.

To further enhance diagnostic performance, this research incorporates multimodal image analysis using both fundus photographs and OCT scans. Retinal abnormalities such as microaneurysms, haemorrhages, and soft exudates are detected from fundus images using a dual-encoder, single-decoder architecture termed “Residual Inception Local Binary Pattern–based Y-Net (RILBP-YNet).” This model combines convolutional feature extraction with

textural analysis through Local Binary Patterns (LBP) computed at multiple radii (1, 3, 5, and 7). The integration of texture-based and deep convolutional features strengthens feature learning and improves the detection accuracy of pathological signs, along with optic disc segmentation. The second major contribution involves depth-wise retinal analysis using OCT imaging to detect fluid accumulation between retinal layers. A U-Net-inspired model, “FAM-U-Net,” is proposed to identify retinal fluid regions. The architecture integrates multiscale feature representations using feature pyramid channels and dilated convolutions to enhance inter-pixel dependencies. Additionally, Convolutional Block Attention Modules (CBAM) and a Deep Aggregation Pyramid Pooling Module (DAPPM) are incorporated to refine salient feature maps and improve localization of fluid regions.

As a third contribution, clinically significant biomarkers such as the Artery-to-Vein Ratio (AVR) and Cup-to-Disc Ratio (CDR) are computed from segmented retinal structures to assist in detecting Hypertensive Retinopathy, Diabetic Retinopathy, and Glaucoma. Furthermore, a transformer-based multimodal deep learning network is developed to generate a unified diagnostic report by jointly analyzing fundus and OCT images through self-attention mechanisms.

Comprehensive qualitative and quantitative evaluations are conducted on multiple public datasets, including INSPIRE-AVR, DRIVE, ORIGA, DRISHTI, UCSD, RETOUCH, OPTIMA, and DUKE, along with real-time clinical datasets collected from eye hospitals. The experimental results demonstrate that the proposed frameworks outperform existing state-of-the-art methods, offering a robust, efficient, and clinically relevant solution for automated retinal disease detection.

सारांश

यह शोध-प्रबंध रेटिना से संबंधित रोगों के व्यापक अध्ययन पर केंद्रित है, जिसमें अपरिवर्तनीय क्षति और दृष्टि हानि को रोकने हेतु प्रारंभिक पहचान पर विशेष बल दिया गया है। ग्लूकोमा, मैक्यूलर एडेमा (ME), हाइपरटेंसिव रेटिनोपैथी (HR), डायबिटिक रेटिनोपैथी (DR) तथा आयु-संबंधी मैक्यूलर डिजनरेशन (AMD) जैसे रेटिनल रोगों का निदान एक महत्वपूर्ण चुनौती बना हुआ है, विशेष रूप से इसलिए क्योंकि प्रारंभिक अवस्था में इनके लक्षण अत्यंत सूक्ष्म होते हैं और पहचानना कठिन होता है। मधुमेह और उच्च रक्तचाप की बढ़ती व्यापकता के कारण रेटिनल रोगों में तीव्र वृद्धि हो रही है, जिससे पहले से ही विशेषज्ञ नेत्र चिकित्सकों की कमी से जूझ रही स्वास्थ्य प्रणालियों पर अतिरिक्त दबाव पड़ रहा है। इस संदर्भ में, स्वचालित चिकित्सा छवि प्रसंस्करण में हालिया प्रगति आशाजनक समाधान के रूप में उभरी है, जो निदान समय को कम करने, मानवीय त्रुटियों को न्यूनतम करने तथा नैदानिक निर्णय प्रक्रिया को समर्थन प्रदान करती है।

इस शोध का मुख्य उद्देश्य गहन अधिगम (डीप लर्निंग) आधारित ऐसे ढांचे विकसित करना है जो रेटिनल छवियों में संरचनात्मक परिवर्तनों और नैदानिक संकेतकों दोनों का पता लगाकर सटीक एवं समयोचित निदान संभव बना सकें। इस अध्ययन में रेटिना के विभिन्न घटकों का विश्लेषण किया गया है, जिनमें रेटिनल रक्त वाहिका मानचित्र, ऑप्टिक डिस्क (OD), ऑप्टिक कप (OC) तथा ऑप्टिकल कोहेरेंस टोमोग्राफी (OCT) स्कैन से प्राप्त रेटिनल द्रव एवं ड्रूज़न जैसी रोगात्मक विशेषताएँ सम्मिलित हैं। संरचनात्मक एवं रोगात्मक विश्लेषण को एकीकृत करके प्रस्तावित प्रणाली प्रारंभिक अवस्था में रोग पहचान की क्षमता तथा रोगी परिणामों में सुधार लाने का लक्ष्य रखती है। यद्यपि इस क्षेत्र में अनेक अध्ययन उपलब्ध हैं, फिर भी स्वचालित प्रणालियों की मजबूती और निर्णय क्षमता को बढ़ाने के संदर्भ में कई शोध अंतराल विद्यमान हैं। इस कार्य का प्रथम प्रमुख योगदान “मल्टीस्टेज DPIRef-Net” नामक एक नवीन बहु-चरणीय द्वि-डिकोडर गहन अधिगम संरचना का विकास है। यह मॉडल रेटिनल रक्त वाहिकाओं का सटीक सेगमेंटेशन करता है तथा उन्हें धमनियों और शिराओं में वर्गीकृत करता है, जिससे निदान में सहायता मिलती है। यह संरचना पूलिंग और स्ट्राइडिंग से जुड़ी सीमाओं को दूर करते हुए निम्न-स्तरीय विशेषताओं के प्रतिनिधित्व को सुदृढ़ बनाती है, जिससे सूक्ष्म रक्तवाहिका विवरण सुरक्षित रहते हैं और धुंधली सीमाओं में कमी आती है। सार्वजनिक रूप से उपलब्ध मानक डेटासेट पर किए गए व्यापक मूल्यांकन प्रस्तावित रक्तवाहिका सेगमेंटेशन ढांचे की मजबूती और सामान्यीकरण क्षमता को दर्शाते हैं। निदान क्षमता को और अधिक बढ़ाने हेतु इस शोध में फंडस फोटोग्राफ तथा OCT स्कैन दोनों का उपयोग करते हुए मल्टीमोडल छवि विश्लेषण को सम्मिलित किया गया है। फंडस छवियों से माइक्रोएन्यूरिज़्म, रक्तस्राव तथा सॉफ्ट एक्सूडेट्स जैसी रेटिनल असामान्यताओं का पता “रेज़िडुअल इनसेप्शन लोकल बाइनरी पैटर्न आधारित वाई-नेट (RILBP-YNet)” नामक द्वि-एन्कोडर, एकल-डिकोडर संरचना द्वारा लगाया जाता है। यह मॉडल कन्वोल्यूशनल विशेषता निष्कर्षण को बहु-त्रिज्या (1, 3, 5 और 7) पर गणना किए गए लोकल बाइनरी पैटर्न (LBP) आधारित टेक्सचर विश्लेषण के साथ संयोजित करता है। टेक्सचर-आधारित तथा गहन कन्वोल्यूशनल विशेषताओं का संयोजन विशेषता अधिगम को सुदृढ़ बनाता है और रोगात्मक लक्षणों की पहचान के साथ-साथ ऑप्टिक डिस्क सेगमेंटेशन की सटीकता में सुधार करता है।

दूसरा प्रमुख योगदान OCT इमेजिंग का उपयोग करते हुए रेटिना की गहराई-आधारित विश्लेषण से संबंधित है, जिसके अंतर्गत रेटिनल परतों के बीच द्रव संचय का पता लगाया जाता है। इस हेतु “FAM-U-Net” नामक U-Net से प्रेरित एक मॉडल प्रस्तावित किया गया है, जो रेटिनल द्रव क्षेत्रों की पहचान करता है। यह संरचना फीचर पिरामिड चैनलों और डाइलेटेड कन्वोल्यूशनों के माध्यम से बहु-पैमाना विशेषताओं को एकीकृत करती है, जिससे पिक्सल-स्तरीय निर्भरताओं में सुधार होता है। इसके अतिरिक्त, कन्वोल्यूशनल ब्लॉक अटेंशन मॉड्यूल (CBAM) तथा डीप एग्रीगेशन पिरामिड पूलिंग मॉड्यूल (DAPPM) को सम्मिलित किया गया है, जिससे महत्वपूर्ण फीचर मैप्स को परिष्कृत किया जा सके और द्रव क्षेत्रों का सटीक स्थानीयकरण संभव हो सके। तीसरे योगदान के रूप में, धमनियों-शिराओं का अनुपात (AVR) तथा कप-टू-डिस्क अनुपात (CDR) जैसे चिकित्सकीय रूप से महत्वपूर्ण बायोमार्कर्स को सेगमेंटेड रेटिनल संरचनाओं से गणना किया गया है, जिससे हाइपरटेंसिव रेटिनोपैथी, डायबिटिक रेटिनोपैथी और ग्लूकोमा की पहचान में सहायता मिलती है। इसके अतिरिक्त, एक ट्रांसफॉर्मर-आधारित मल्टीमोडल डीप लर्निंग नेटवर्क विकसित किया गया है, जो सेल्फ-अटेंशन तंत्र के माध्यम से फंडस और OCT छवियों का संयुक्त विश्लेषण कर एक एकीकृत नैदानिक रिपोर्ट तैयार करता है।

INSPIRE-AVR, DRIVE, ORIGA, DRISHTI, UCSD, RETOUCH, OPTIMA और DUKE सहित अनेक सार्वजनिक डेटासेट्स के साथ-साथ नेत्र चिकित्सालयों से प्राप्त वास्तविक नैदानिक डेटासेट्स पर व्यापक गुणात्मक एवं मात्रात्मक मूल्यांकन किए गए हैं। प्रायोगिक

परिणाम यह दर्शाते हैं कि प्रस्तावित ढांचे वर्तमान अत्याधुनिक विधियों की तुलना में बेहतर प्रदर्शन करते हैं और स्वचालित रेटिनल रोग पहचान के लिए एक सुदृढ़, प्रभावी एवं चिकित्सकीय रूप से उपयोगी समाधान प्रदान करते हैं।

Table of Contents

CERTIFICATE	ii
Acknowledgements.....	iii
<i>Abstract</i>	v
List of Figures	xii
List of Tables	xix
List of abbreviations	xxii
1.1 EPIDEMIOLOGY OF RETINAL DISORDERS.....	1
1.2 HUMAN EYE ANATOMY.....	4
1.2.1 STRUCTURAL ANATOMY OF THE EYE.....	4
1.2.2 ANALYSIS OF RETINAL IMAGING IN CLINICAL DIAGNOSIS AND RESEARCH.....	6
1.3 IRREVERSIBLE VISUAL COMPLICATIONS.....	9
1.3.1 DIABETIC RETINOPATHY.....	9
1.3.2 GLAUCOMA.....	12
1.3.3 HYPERTENSIVE RETINOPATHY.....	14
1.3.4 MACULAR COMPLICATIONS.....	15
1.3.5 DETECTION METHODS FOR RETINAL DISORDERS.....	17
1.4 LITERATURE SURVEY.....	18
1.4.1 BLOOD VESSEL, OD, AND OC SEGMENTATION.....	19
1.4.2 LESION SEGMENTATION.....	20
1.4.3 DETECTION OF RETINAL FLUIDS.....	20
1.5 RESEARCH GAPS.....	22
1.5.1 LIMITED DIVERSITY AND GENERALIZABILITY OF RETINAL DATASETS.....	22
1.5.2 ROBUSTNESS TO IMAGE QUALITY VARIATIONS.....	22
1.5.3 LIMITED MULTIMODAL DATA INTEGRATION:.....	23
1.5.4 INADEQUATE EXTRACTION OF SIGNIFICANT FEATURE INFORMATION:.....	23
1.5.5 LACK OF EXPLAINABILITY IN AI MODELS:.....	24
1.6 MOTIVATION.....	24
1.7 THESIS LAYOUT.....	25

2.2 INSIGHT INTO PROPOSED RESEARCH WORK.....	30
2.3 CLASSIFICATION AND LOCALIZATION OF RETINAL VESSELS	31
2.3.1 ENHANCEMENT OF INPUT IMAGES USING PRE-PROCESSING STEPS	32
2.3.2 DEVELOPMENT OF ROBUST MULTISTAGE DPIREF-NET	33
2.3.2.1 Overall Network Design	34
2.3.2.2 Multiscale Feature Extraction and Feature Categorization	34
2.3.2.3 Up-sampling and output feature maps generation	35
2.3.2.4 INTERACTIVE MULTISTAGE REFINEMENT.....	36
2.3.3 A ROBUST GUIDED FILTERING FOR VESSEL MAP EXTRACTION.....	37
2.4 LESION SEGMENTATION	38
2.4.1. PRE-PROCESSING STAGES AND EXTRACTION OF LBP	40
2.4.1.1 Local Binary Patterns.....	41
2.4.2. IMPLEMENTATION OF RILBP-YNet	42
2.4.2.1 Application of RILBP encoder	43
2.4.2.2 Deployment of decoder.....	44
2.5 EXPERIMENTS AND RESULTS FOR VESSEL CLASSIFICATION	44
2.5.1. DATASET DESCRIPTION	44
2.5.2. THE TRAINING DETAILS OF DEVELOPED MULTISTAGE DPIREF-NET FRAMEWORK	47
2.5.2.1 Weighted Loss function values for updating the weights	47
2.5.2.2 Quantitative measures for evaluation of developed model	49
2.5.3. STUDIES FOR ESTIMATING SIGNIFICANCE OF EACH COMPONENT.....	51
2.5.4. COMPARATIVE ANALYSIS OF THE MULTISTAGE DPIREF-NET WITH THE EXISTING NETWORKS AND METHODOLOGIES.....	53
2.5.5. ROBUSTNESS OF THE DEVELOPED NETWORK ON VARIOUS DIVERSE DATASETS.	54
2.6 EXPERIMENTAL RESULTS FOR LESION AND OD SEGMENTATION	55
2.6.1. DATASET DESCRIPTION	55
2.6.2. DESIGN AND EXECUTION OF THE DEVELOPED RILBP-YNET FRAMEWORK.....	56
2.6.3. ANALYSIS OF THE SEGMENTATION OUTPUTS.....	59
2.6.4. QUANTITATIVE COMPARISON ANALYSIS OF DEVELOPED MODEL	61
2.6.4.1. Comparative analysis of developed network against top teams of IDRiD Challenge	61

2.6.4.2. The comparative performance analysis between the proposed RILBP-YNet and various existing methods over different datasets.....	62
2.6.5. SIGNIFICANCE OF EACH COMPONENT IN DEVELOPED RILBP-YNET	65
2.7 CONCLUSIONS.....	67
3.1 INTRODUCTION	69
3.2 INSIGHT INTO PROPOSED RESEARCH WORK.....	71
3.3 PROPOSED METHODOLOGY	72
3.3.1 PRE-PROCESSING STEPS FOR IMAGE ENHANCEMENT.....	72
3.3.2 DESIGN AND DEVELOPMENT OF FAM-U-NET FRAMEWORK.....	73
3.3.2.1. Multiscale Contextual Feature Analysis Module.....	75
3.3.2.2. Deep Feature Fusion Block.....	76
3.3.2.3. WEIGHTED LOSS FUNCTION.....	76
3.4 MODEL DEPLOYMENT AND EVALUATION FRAMEWORK.....	77
3.4.1 DATASET DESCRIPTION	77
3.4.2 EXPERIMENTAL SETUP FOR TRAINING OF FAM-U-NET.....	79
3.4.4 EVALUATION OF FAM-U-NET’S PERFORMANCE OVER DIFFERENT DATASETS.....	83
3.4.4 EVALUATION OF FAM-U-NET’S PERFORMANCE OVER EXISTING METHODS.....	87
3.4.5 COMPUTATIONAL TIME AND LIMITATIONS	88
3.4.5 CONCLUSION.....	88
4.1 INTRODUCTION	90
4.2 INSIGHT INTO PROPOSED RESEARCH WORK.....	93
4.3 PROPOSED METHODOLOGY	94
4.3.1 DETECTION OF RETINAL VESSELS USING HYBRID RA2 -NET.....	94
4.3.1.2. Channel Attention Module.....	96
4.3.1.3. Implementation of Decoder	97
4.3.2 LOCALIZATION OF RETINAL VESSELS USING SAF-NET	97
4.3.2.1. Multiscale Feature Fusion (MSFF).....	98
4.3.2.2. The framework of ResNest Block.....	100
4.3.2.3. Implementation of Decoder of SAF-Net.....	100
4.3.3 AVR ESTIMATION USING Sequential ARL-SegNet.....	100
4.3.3.1 Pre-processing.....	101
4.3.3.2 Encoder Implementation of the Sequential ARL-SegNet.....	102

4.3.3.3 Decoder Implementation of the Sequential ARL-SegNet.....	104
4.3.3.4 Computation of AVR value from segmented vessel maps	105
4.3.4 CDR ESTIMATION	106
4.3.4.1 Encoder Implementation	106
4.3.4.2 Decoder Implementation.....	107
4.3.4.3 CDR estimation using OD and OC maps.....	108
4.4 EXPERIMENTAL RESULTS.....	108
4.4.1 VESSEL SEGMENTATION RESULTS USING HYBRID RA ² -NET	108
4.4.1.1 Datasets and corresponding pre-processing techniques	108
4.4.1.2 Hyperparameter tuning and training strategy.....	109
4.4.1.3 Segmentation Results using the Hybrid RA ² -Net	110
4.4.2 VESSEL CLASSIFICATION RESULTS USING SAF-NET.....	111
4.4.2.1 Datasets	111
4.4.2.2 Training strategy and hyperparameter optimization of SAF-Net.....	112
4.4.2.3 Segmentation Results of SAF-Net	112
4.4.3 ESTIMATION OF AVR RESULTS	115
4.4.3.1 Datasets	115
4.4.3.2 Implementation of the Sequential ARL-SegNet	116
4.4.3.3 Comparison of the proposed Sequential ARL-SegNet with Baseline models	117
4.4.3.4 Gradation of HR and Comparison of the proposed method with existing methods and datasets.....	119
4.4.4 ESTIMATION OF CDR RESULTS USING ALWRes-Net	121
4.4.4.1. Datasets	122
4.4.4.2 Training and Fine-tuning of network parameters.....	122
4.4.4.3 Comparison of Segmentation Results of ALWRes-Net.....	124
4.5 CONCLUSIONS.....	124
5.1 INTRODUCTION	127
5.2 INSIGHT INTO PROPOSED RESEARCH WORK.....	129
5.3 PROPOSED METHODOLOGY	130
5.3.1 TRANSFORMER EMBEDDED ENCODER BLOCK (TEEB).....	130
5.3.2 IMPLEMENTATION OF MSRF SUBNETWORK	132
5.3.3 DECODER ALONG WITH SCA.....	136

5.4 EXPERIMENTAL SETUP OF TMRF-NET	136
5.4.1 DESCRIPTION OF INPUT DATA	137
5.4.2 IMPLEMENTATION SETUP AND TRAINING PROCESS OF TMRF-NET	138
5.4.2.1. Loss function.....	138
5.5 DISCUSSION ON RESULTS OF TMRF-NET	139
5.5.1 ABLATION STUDIES.....	140
5.5.2 COMPARISON OF THE TMRF-NET WITH THE EXISTING METHODS.....	140
5.5.3 EVALUATION OF DEVELOPED TMRF-NET EFFICACY ON DIFFERENT DATASETS. 141	
5.5.3.1 Performance of TMRF-Net on RETOUCH dataset	142
5.5.3.2 Segmentation on other modalities	143
5.6 COMPUTATIONAL TIME	144
5.7 CONCLUSIONS.....	145
6.1 MAIN CONCLUSIONS	146
6.2 FUTURE DIRECTIONS	148
List of Publications	150
Bibliography:	152
Bibliography of the Author:.....	168

List of Figures

Fig.1.1	Global estimates of people suffering from different eye conditions [6]	2
Fig.1.2	Global estimates of people suffered from AMD and Glaucoma between 2016 to 2030 [6]	2
Fig.1.3	Regional estimates of people suffering from AMD and Glaucoma [6]	3
Fig.1.4	(a) Anatomical structure representation of the eye (b) Depth-wise layers of the retina.	5
Fig.1.5	Layer-wise view of the Retinal surface of the eye illustrating different retinal layers of the eye	6
Fig.1.6	(a) Fundus scan of the retina (b) Fundus scan with different lesions	6
Fig.1.7	(a) A sample OCT scan without Macular Edema (b) A sample OCT scan with Macular Edema from the RETOUCH dataset	8
Fig.1.8	Normal Vision vs. DR-affected Vision	10
Fig.1.9	Animated fundus images with NPDR and PDR cases	10
Fig.1.10	Retinal Image with new blood vessels on the disc (NVD) and elsewhere (NVE)	11
Fig.1.11	The anatomical structure of the eye illustrates drainage pathways [30]	13
Fig.1.12	(a) Open-angle Glaucoma (OAG) (b) Closed-angle Glaucoma (CAG)	13
Fig.1.13	Typical Fundus images that show HR symptoms	15
Fig.2.1	(a) A sample fundus image from the AVRDB dataset (b) Pixel annotated label of vascular map (c) Pixel annotated label of arteriolar vascular map(d) Pixel annotated label of venular vascular map.	29
Fig.2.2	A random fundus image (left) was selected from the IDRiD dataset along with its annotated label (right). The color on the label indicates red, blue, yellow, green, and white representing hemorrhages, microaneurysms, soft exudates, hard exudates, and OD respectively.	29
Fig.2.3	(a) Green channel of sample fundus image of AVRDB dataset (b) Filtered outcome of (a) using Gaussian filter, (c) Contrast enhancement of (b), (d) Enhanced image of (c) using Gamma correction	32
Fig.2.4	The structural design of the proposed Multistage DPIRef-Net for retinal vessel classification	33
Fig.2.5	Inception module integrated with U-Net	34

Fig.2.6	Workflow of the proposed guided filtering technique (a) Original retinal image (b) Edge probability map generated by the proposed Multistage DPIRef-Net, (c) Corresponding regional probability map (d) Final refined regional vascular map after applying the guided filtering technique. Arrow annotations highlight significant improvements in edge continuity and the suppression of false positives in non-vascular regions, demonstrating the effectiveness of the post-processing step.	37
Fig.2.7	The series pre-processing steps employed to perform on the retinal image prior to model input. A sequence of enhancement and transformation steps is performed on original input image, including extraction and enhancement of the green channel for computing the LBPs.	40
Fig.2.8	The novel architecture of the proposed RILBP-YNet with a depth of 4	42
Fig.2.9	The structural flow of RI-LBP-YNet's encoder	43
Fig.2.10	The structure of the RI module of Encoder	43
Fig.2.11	The architecture of RILBP-YNet's decoder	44
Fig.2.12	The estimation process of edge-level pixel level annotated labels (a) resized region-based annotated label (b) the dilated version of the region-based annotated label (c) Extracted edge obtained by subtracting (a) from (b)	45
Fig.2.13	The effectiveness of developed Multistage DPIRef-Net assessed during training process using the (a) weighted loss function vs epochs and (b) the Dice coefficient vs epochs	45
Fig.2.14	Receiver Operator characteristics (ROC) curves obtained from the backbone model along with the proposed Multistage DPIRef-Net during evaluation process (a) ROC curve for veins segmentation (b) ROC curve for arteries segmentation.	49
Fig.2.15	The segmentation results of proposed model on randomly selected fundus images from the AVRDB dataset (a) Original fundus image, (b) edge map emphasizing arterial structures, (c) edge map emphasizing venous structures, (d) regional-based artery segmentation, (e) regional-based veins segmentation map (f) final combined vascular map refined using guided filtering, with arteries shown in red and veins in green.	50
Fig.2.16	Mean error bar plots comparing the F1 scores of arteries and vein segmentation between the baseline backbone model and developed Multistage DPIRef-Net, with a significance level of 0.05.	52
Fig.2.17	Illustration of the segmented outcomes of arterial and venous structures detected by various models (a) segmented edge vascular maps of artery (b) segmented edge vascular maps of vein (c) regional-based arteries segmentation map (d) regional-based vein segmentation map. first row displays the segmentation outcomes of U-Net, whereas,	53

- the second, third and last row corresponds to the segmentation outputs of RU-Net, CRU-Net, and developed Multiscale DPIRef-Net respectively.
- Fig.2.18 Pre-processing stages of an input fundus image from the IDRiD dataset, (a) Resized fundus scan, (b) green channel extraction, (c) Enhanced outcome after applying CLAHE on (b) and, (d) the final outcome after gamma correction on (c). 56
- Fig.2.19 Local Binary Pattern (LBPs) computed from pre-processed fundus scan at different radi 1, 3, 5 & 7 displayed sequentially from left to right and top to bottom. 56
- Fig.2.20 AUPR curves of lesions, such as Microaneurysms (MA), Soft Exudates (SE), Haemorrhages (HE), Hard Exudates (EX), and Optic Disc (OD) are computed using the IDRiD dataset 57
- Fig.2.21 Training Performance of RILBP-Ynet evaluated using (a) Dice score vs epochs, (b) Loss function value vs epochs, (c) Sensitivity vs epochs, and (d) Specificity vs epochs 58
- Fig.2.22 Box Plot visualization of sensitivity of each lesion type and OD, evaluated on the IDRiD dataset 58
- Fig.2.23 Dice Coefficients achieved by the developed model for individual lesion and OD segmentation from the fundus scans of IDRiD dataset 60
- Fig.2.24 Segmented outputs of fundus scans from IDRiD dataset alongside with the standard pixel-level annotated labels and predicted probabilistic labels (from left to right). 60
- Fig.2.25 Visualization of feature maps from the decoder layers of RILBP-Ynet progressing from deeper to shallower levels (left to right). The top row indicates the decoder feature maps before incorporating with LBP encoder outputs, while the bottom row illustrates the enhanced features after fusion with LBP-derived information 62
- Fig.2.26 Comparative visualization of segmentation results between the proposed model and existing methods as per [142] (a) Input fundus image (b) standard ground truth label, segmented results of (c) HED network, (d) FCRN (e) CASNet architecture (f) DeepLab v3+ (g) L-seg, and (h) the proposed RILBP-YNet 62
- Fig.2.27 Random sample images from various datasets including DRIVE, CHASE, STARE, and locally captured real-time images used for qualitative evaluation of the proposed RILBP-YNet (a) Input retinal image from each dataset (b) Corresponding segmented outputs of (a) detected by proposed model 64
- Fig.2.28 Ablation study evaluating the impact of Local Binary Patterns (LBP) and architectural components (a) Input Image (b) Standard ground truth label, Segmentation results from (c) Residual block with LBP (d) Residual block without LBP (e) Inception module with LBP (f) Inception module without LBP (g) The complete RILBP architecture 65

Fig.2.29	Ablation Study demonstrating the effect of different loss functions on segmentation performance (a) Fundus image (b) Standard ground truth label (c) Prediction using CCE (d) Prediction using JL (e) Prediction using a weighted linear combination of JL and CCE losses.	66
Fig.3.1	Workflow of pre-processing steps for OCT scans (a) Original 2D OCT image (b) OCT scan obtained after noise reduction (c) Region of Interest (ROI) cropped OCT image	73
Fig.3.2	The overview of the complete FAM-U-Net model architecture	74
Fig.3.3	Training and validation performance FAM-U-Net on the RETOUCH dataset shown across epochs for various metrics (a) Dice score, (b) Sensitivity, (c) Specificity, (d) Accuracy, (e) Loss.	80
Fig.3.4	Calibration plot illustrating the probabilistic predictions of the proposed model for different types of retinal fluid segmentation.	81
Fig.3.5	Comparative visualization of segmentation results, (a) Resized OCT image (b) Annotated ground truth, (c) U-Net output, (d) U-Net enhanced with MFE and SE blocks, (e) U-Net integrated with CBAM, (f) U-Net with DAPPM module, (g) the output of the FAM-U-Net model.	82
Fig.3.6	Segmentation predictions of FAM-U-Net on the OPTIMA dataset, (a) Resized OCT image, (b) Corresponding ground truth label, (c) Predicted segmentation by FAM-U-Net.	84
Fig.3.7	Performance of FAM-U-Net on the DUKE dataset (a) Resized OCT image, (b) Corresponding ground truth, (c) Predicted segmentation from FAM-U-Net.	85
Fig.3.8	Bar chart displaying mean error in segmenting individual retinal fluid types using FAM-U-Net on the RETOUCH dataset.	86
Fig.3.9	ROC curve representing the diagnostic capability of FAM-U-Net in detecting the retinal fluids from OCT scans in the RETOUCH dataset.	86
Fig.4.1	The structural layout of the Hybrid RA ² -Net model	95
Fig.4.2	Internal configuration of the residual hybrid atrous convolution module	96
Fig.4.3	Architecture of the channel attention mechanism	96
Fig.4.4	Framework of the recurrent convolutional block	96
Fig.4.5	The entire architecture of SAF-NET tailored for retinal vascular detection	97
Fig.4.6	The structural flow of MSFF module in SAF-Net	98
Fig.4.7	The internal components of the ResNest block employed in SAF-Net. (a) ResNest architecture (b) Cardinal block structure (c) Split attention mechanism	99
Fig.4.8	The architecture of Sequential ARL-SegNet	101

Fig.4.9	The encoder of Sequential ARL	103
Fig.4.10	The ARL block in encoder of proposed ARL SegNet	103
Fig.4.11	The process of computing vessel width from arteries and veins accordingly (a) Vascular map (b) Skeletonized vascular map (c) Branch pixel points extended to 10 pixels (d) Detected vessel segments for vessel width estimation.	105
Fig.4.12	The architecture of developed ALWRes-Net for localization of OD and OC pixels in fundus images	106
Fig.4.13	Workflow of Attention Mechanism in developed ALWRes-Net	107
Fig.4.14	The CDR estimation process using the bounding boxes from the binary masks of OC and OD	107
Fig.4.15	Visualization of retinal vascular map segmentation by the Hybrid RA ² -Net on the AV dataset and DualMode 2019 datasets. (a) Resized fundus image (b) Manully annotated artery map (c) Predicted artery segmentation, (d) Manually annotated vein map, and (e) Predicted vein segmentation.	110
Fig.4.16	Retinal vessel segmentation performance of Hybrid RA ² -Net on the DRIVE dataset. (a) Resized fundus image (b) Reference vessel masks (c) Model predicted vessel masks	110
Fig.4.17	Model training progression SAF-Net during first 200 epochs, showing changes in Dice coefficient and loss value to evaluate learning stability and accuracy.	111
Fig.4.18	Output of SAF-Net on DualMode 2019 and AV test subsets, (a) Resized fundus image (b) Ground truth of arterial vessels (c) Arterial prediction (d) Ground truth of venous vessels, and (e) Venous prediction mask.	112
Fig.4.19	Prediction outcomes from SAF-Net using a locally collected retinal dataset, (a) Input fundus image, (b) segmentation results for arteries and (c) segmentation result for veins	114
Fig.4.20	An Image from the AVRDB dataset with respective ground truths (a)fundus image (b) articular vascular map (c) Venular Vascular map (d) total vascular map	114
Fig.4.21	Image enhancement and pre-processing pipeline for AVRDB dataset. (a) Raw fundus image (b) Green channel extraction (c) CLAHE-enhanced image amplified by a clip limit of 1.7, and (d) Output after applying a modified SUACE method.	115
Fig.4.22	The robustness of the proposed network in terms of various metrics like Sensitivity, Specificity, Dice coefficient, linear combined loss value, and Accuracy with respect to epochs	116
Fig.4.23	Segmentation outcomes of the developed model (1 st and 3 rd rows of the original images (input image, arteriolar vessel map, venular vessel map) left to right. 2 nd and 4 th rows	117

the pre-processed and segmented images (pre-processed input image, predicted arteriolar vessel map, predicted venular vessel map) left to right.

Fig.4.24	The significance of linear combined loss function values on the proposed network	118
Fig.4.25	ROC curves of the Proposed Sequential ARL-SegNet	118
Fig.4.26	Activation maps of attention masks of lower layers at each encoder block (a) Activation maps at the end of 1 st encoder (b) Activation maps at the end of 2 nd encoder (c) Activation maps at the end of 3 rd encoder (d) Activation maps at the end of last encoder	120
Fig.4.27	Training performance of the developed model for 200 epochs (a) Dice coefficient (b) Loss function values	122
Fig.4.28	Predicted segmentation masks of proposed ALWResNet obtained from various datasets (a) ORIGA (b) DRISHTI-GS1 (c) REFUGE (d) Rim-One V3	123
Fig.5.1	The entire architecture of TMRF-Net for multiclass segmentation retinal fragments and abnormalities	130
Fig.5.2	The structural flow of the TEEB module for feature extraction	131
Fig.5.3	(a) DPDSF block (b) MSRF-subnetwork with feature maps ($X_{n,s}$) at the n th block with s scales	133
Fig.5.4	Structure of Spatial-wise Cross Attention module for mitigating pixel discrepancies	134
Fig.5.5	The impact of each module on developed TMRF-Net (a) Sample B-scan (b) Ground truth (c) U-Net (d) U-Net enhanced with TEEB (e) U-Net connected with MSRF (f) U-Net improved with MSRF and SCA (g) TEEB integrated with MSRF (h) U-Net+ MSRF + SCA (i) TEEB + SCA (j) proposed TMRF-Net	139
Fig.5.6	Segmentation maps of drusens on a random OCT image in UCSD dataset (a) OCT image (b) Ground truth (c) Att-UNet (d) U-Net (e) MsTGA-Net (f) Proposed TMRF-Net	140
Fig.5.7	Output feature maps of proposed TMRF-Net with Grad-CAM (a) Input Image (b) Grad-CAM of 1 st layer (c) Grad-CAM of 1 st encoder (d) Grad-CAM of 2 nd encoder (e) Grad-CAM of 1 st decoder (f) Grad-CAM of 2 nd decoder (g) Grad-CAM of 3 rd decoder (h) Grad-CAM of last layer convolutional layer	142
Fig.5.8	Box plots of Dice score values for each fluid of the RETOUCH dataset	142
Fig.5.9	Segmentation outcomes of developed TMRF-Net on RETOUCH dataset (a) Sample OCT image (b) Ground image of all fluids (c) Predicted map of all fluid (d) Predicted map of IRF (e) Predicted of SRF (f) Predicted map of PED (red indicates the IRF, green indicates SRF and blue indicates PED fluid)	142

- Fig.5.10 Segmentation results of proposed TMRF-Net on INSPIRE and ORIGA dataset (a) 143
Sample OCT image (b) Ground image of OD/arteries (c) Ground image of OC/veins
(d) Predicted of OD/arteries (e) Predicted map of OC/veins (the first rows indicate the
segmentation results of blood vessels from INSPIRE dataset and last rows indicates the
segmentation maps of OC and OD from ORIGA dataset)
- Fig.5.11 Segmentation results of OD and OC from retinal images real-time private dataset 144
collected from our collaborating hospital

List of Tables

Table 2.1	The details of layers at each refinement stage of the proposed Multistage DPIRef-Net	35
Table 2.2	Distribution of the number of pixels for each type of lesion on retinal images of the IDRiD dataset	39
Table 2.3	The detailed summary of training and testing sets of all datasets	46
Table 2.4	The detailed evaluation of the effectiveness of each component in the overall performance of the proposed model on the AVRDB dataset (The highest metrics in each column are indicated in bold letters)	51
Table 2.5	Comparative analysis between the proposed model and other existing state-of-the-art methodologies for performing the task of detecting arteries and veins vascular maps. (The highest metrics in each column are indicated in bold letters)	52
Table 2.6	The comparative analysis proposed the model's performance in segmenting vascular maps from different datasets in terms of various quantitative metrics	54
Table 2.7	Quantitative performance metrics of the proposed RILBP-YNet model for individual lesion classes on the IDRiD dataset, evaluated using a uniform threshold of 0.5	59
Table 2.8	AUC value comparison between the proposed model and the top teams of IDRiD Challenge Teams [139].	61
Table 2.9	Comparison analysis of AUC scores of proposed methods with Baseline Models as per [142].	63
Table 2.10	Quantitative analysis of the developed model with existing models using the IDRiD dataset [139].	63
Table 2.11	Quantitative analysis of the developed model with baseline models using the e-ophta dataset	64

Table 2.12	Ablation Study results demonstrating the contribution of individual components in the proposed RILBP-YNet, evaluated on the IDRiD dataset. Metrics include Dice coefficient, number of parameters and training duration. (Bold values represents the best values)	65
Table 2.13	Ablation Study analyzing the effect of different loss functions on the performance of the proposed RILBP-YNet, evaluated using the IDRiD dataset based on Dice coefficient. (Bold values represent the best performance metric)	66
Table 2.14	Quantitative evaluation comparing Serial (S) and parallel (P) configurations of convolutional layers within the encoder block of proposed RILBP-YNet.	66
Table 3.1	Ablation analysis to depict the significance of each component of the developed FAM-U-Net (the best values are highlighted in Bold)	83
Table 3.2	Quantitative evaluation of developed FAM-U-Net for segmenting retinal fluids across various vendors in the RETOUCH dataset using significant metric values	83
Table 3.3	Assessment of the FAM-U-Net model's effectiveness in segmenting IRF from OCT scans in the OPTIMA and DUKE based on various key evaluation metric values	84
Table 3.4	Performance comparison between FAM-U-Net and existing models across multiple vendors in the RETOUCH dataset-based Dice coefficient values.	87
Table 3.5	Evaluation of the proposed FAM-U-Net against earlier methodologies for segmenting IRF in the OPTIMA dataset.	88
Table 3.6	Evaluation of the proposed FAM-U-Net with earlier methodologies for segmenting IRF in the DUKE dataset	88
Table 4.1	Relation Between AVR and HR	92
Table 4.2	The segmentation results of the proposed Hybrid RA^2 -Net with existing methodologies in terms of different metrics when evaluated using the AV dataset.	109
Table 4.3	The effectiveness of developed Hybrid RA^2 -Net over different diverse datasets in terms of quantitative metrics.	109
Table 4.4	Comparison results of proposed SAF-Net with existing models using the segmentation results obtained using the DualModel2019 dataset	113

Table 4.5	The performance metrics of the proposed SAF-Net for different datasets in detecting arteries and veins	113
Table 4.6	Comparison of proposed Sequential ARL-SegNet with Baseline Networks in segmenting arteries and veins	118
Table 4.7	Validation of the proposed model using Different Datasets	121
Table 4.8	Comparison of the Proposed algorithm with previous methods	121
Table 4.9	Impact of each module of the proposed network for the segmentation of arteries and veins	121
Table 4.10	Summary of the databases used in the proposed work.	121
Table 4.11	Quantitative analysis of the proposed model on various standard datasets	123
Table 4.12	Quantitative comparison of the proposed model with previous models	123
Table 5.1	The significance of each module in comparison with the proposed model when tested on the UCSD dataset (Bold letters indicate the highest values of each column)	139
Table 5.2	Comparison of proposed model with existing models using UCSD dataset.	141
Table 5.3	Quantitative results of the proposed model on different datasets	144

List of abbreviations

ME	Macular Edema
HR	Hypertensive Retinopathy
DR	Diabetic Retinopathy
AMD	Age-related Macular Degeneration (AMD)
OD	Optic Disc
OC	Optic Cup
OCT	Optical Coherence Tomography
CBAM	Convolutional Block Attention Modules
DAPPM	Deep Aggregation Pyramid Pooling Module
AVR	Arteries-to-Veins Ratio
CDR	Cup-to-Disc Ratio
WHO	World Health Organization
CDCP	Centers for Disease Control and Prevention
RE	Refractive Error
IAPB	International Agency for the Prevention of Blindness
CAD	Computer Aided Diagnosis
RPE	Retinal Pigment Epithelium
PL	Photoreceptor Layer

ELM	External Limiting Membrane
ONL	Outer Nuclear Layer
OPL	Outer Plexiform Layer
INL	Inner Nuclear Layer
IPL	Inner Plexiform Layer
GCL	Ganglion Cell Layer
NFL	Nerve Fiber Layer
ILM	Inter Limiting Membrane
FOV	Field of View
ONH	Optic Nerve Head
SD-OCT	Spectral Domain OCT
PED	Pigment Epithelium Detachment (PED)
SRF	Sub Retinal Fluid
IRF	Intra Retinal Fluid
NPDR	Non-Proliferative Diabetic Retinopathy
PDR	Proliferative Diabetic Retinopathy
NVD	Neovascularization on Optic Disc (NVD)
NVE	Neovascularization Elsewhere (NVE)
IDF	International Diabetes Federation
IOP	Intraocular Pressure
ARIC	Atherosclerosis Risk in Communities

OAG	Open-Angle Glaucoma (OAG)
CAG	Closed-Angle Glaucoma (CAG)
RVO	Retinal Vein Occlusion
DME	Diabetic Macular Edema
CME	Cystoid Macular Edema
MA	Microaneurysms
HE	Hemorrhages
EX	Hard Exudates
SE	Soft Exudates
LSSVM	Least Square Support Vector Machines
GMM	Gaussian Mixture Models
SVM	Support Vector Machine
LDA	Linear Discriminant Analysis
SGRIF	Structure-Preserving Guided Retinal Image Filtering
FCM	Fuzzy C-Means
CNN	Convolutional Neural Network
DCNN	Deep Convolutional Neural Network
FCNN	Fully Convolutional Neural Network
AI	Artificial Intelligence
CLAHE	Contrast Limited Adaptive Histogram Equalization
SUACE	Speed Up Adaptive Contrast Enhancement
CAM	Class Activation Maps

LBP	Local Binary Patterns
BCE	Binary Cross Entropy
ACC	Accuracy
SEN	Sensitivity
SP	Specificity
MCC	Mathew's Correlation Coefficient (MCC)
DC	Dice Coefficient
ROC	Receiver Operating Characteristics
AUC	Area Under the Curve
ISBI	International Symposium on Biomedical Imaging
PSNR	Peak Signal-to-Noise Ratio
AUPR	Area Under Precision-Recall Curve
NSR	Neuro-Sensory Retina
MFE	Multiscale Feature Extraction
LN	Layer Normalization
GeLU	Gaussian Error Linear Unit
BM3D	Block Matching and 3D Filtering
FP	Feature Pyramid
SEB	Squeeze and Excitation Block
GAP	Global Average Pooling
RoI	Region of Interest
WCE	Weighted Cross Entropy

GPU	Graphical Processing Unit
STAPLE	Simultaneous Truth and Performance Level Estimation
SLO	Scanning Laser Ophthalmoscopy
NRR	Neuro-Retinal Rim
RHAC	Residual Hybrid Atrous Convolution
RCM	Recurrent Convolution Modules
SAF	Split Attention-Fusion
MSFF	Multiscale Feature Fusion
ARL	Attention Residual Learning
CRVE	Central Retinal Venular Equivalent
CRAE	Central Retinal Artery Equivalent
DPDSF	Dual Path Dual Scale Fusion
TMRF	Transformer Encoder-based Multiscale Residual Fusion
TEEB	Transformer Embedded Encoder Block
MSRF	Multiscale Residual Fusion
GTB	Global Transformer Block
RNFL	Retinal Nerve Fiber Layer
UCSD	University of California San Diego
JL	Jaccard Loss